Available online at www.sciencedirect.com
ScienceDirect
Journal of Molecular Catalysis A: Chemical 264 (2007) 170–178
JOURNAL OF MOLECULAR CATALYSIS A: CHEMICAL
www.elsevier.com/locate/molcata

In situ generation of Pd nanoparticles in MCM-41 and catalytic applications in liquid-phase alkyne hydrogenations

Ágnes Mastalir[a,*], Bulcsú Rác[a], Zoltán Király[b], Árpád Molnár[a]

[a] *Department of Organic Chemistry, University of Szeged, H-6720 Szeged, Dóm tér 8, Hungary*
[b] *Department of Colloid Chemistry, University of Szeged, Aradi vt. 1, H-6720 Szeged, Hungary*

Received 31 May 2006; received in revised form 9 August 2006; accepted 14 September 2006
Available online 16 September 2006

Abstract

Pd–MCM-41 materials were synthetized by using the cationic surfactant tetradecyltrimethylammonium bromide (C_{14}TABr) for both the stabilization of the Pd particles and the construction of the mesoporous structure of MCM-41. Two Pd–MCM-41 samples, for which the Pd particles were generated before and after formation of the MCM-41 framework (Pd-A and Pd-B, respectively), were investigated. Structural characterization of the samples was carried out by ICP-AES, N_2 sorption, XRD and TEM measurements. It was established that the highly ordered structure of MCM-41 was not appreciably affected by the formation of the Pd particles. Further, a similar particle size control was achieved for both Pd–MCM samples. However, both the location and the size distribution of the Pd particles were found to depend strongly on the preparation procedure. For Pd-A, the Pd nanoparticles were essentially situated on the external surface of MCM-41, whereas for Pd-B, the particles were found to be encapsulated inside the mesopores. For the liquid-phase hydrogenations of alkynes, the catalytic activity of Pd-A clearly surpassed that of Pd-B, indicating that the external Pd crystallites were more readily accessible for the reactants than those incorporated in the MCM-41 framework. The limited activity observed for Pd-B was attributed to mass transport limitations due to diffusion of the reactants into the mesopores of the MCM-41 host.

Keywords: Palladium; MCM-41; Cationic surfactant; N_2 sorption; X-ray diffraction; Transmission electron microscopy; Encapsulation; Alkyne hydrogenation; Turnover frequency; Selectivity

1. Introduction

Since their discovery in the early 1990s, ordered mesoporous materials, including MCM-41, have been the subject of an extended research, mainly in terms of their syntheses, synthesis modifications and applications in the fields of adsorption, separation, host–guest type interactions and catalysis [1–5]. The favourable properties of MCM-41 comprise a regular pore system (hexagonally shaped pores with a uniform size of 2–10 nm in nonintersecting straight channels), a high specific surface area ($\sim$1000 $m^2\ g^{-1}$) and an enhanced thermal stability [3,4,6]. The surface properties of MCM-41 can also be modified by the incorporation of B, Ti or V atoms, and the mesopores tend to accommodate various complexes or reactant molecules [2,3,7,8]. It follows that MCM-41 can be widely employed for a number of catalytic reactions, either as a catalyst or as a host material for metal complexes or nanoparticles [2,9–11]. As related to their acidity, MCM-41 materials have long been utilized for cracking and hydrocracking reactions [9], whereas doped or organically modified MCM-41s have found various applications in the field of organic catalysis [2,12,13].

MCM-41 is typically synthetized from a silica source and a cationic alkyl ammonium surfactant via a micelle-based liquid crystal templating mechanism [1] at a variety of pH values, at concentrations under which micelle formation is favourable. This method implies the formation of a surfactant-rich precipitate and thus templating occurs in a heterogeneous gel phase [14,15]. Other procedures, based on the application of neutral or anionic surfactants, resulting in the formation of MCM-41-like structures of lower crystallinity, have also been reported [2,9,15,16]. Several methods have been published in the literature for the preparation of MCM-41 supported metal nanoparticles, including the incipient wetness impregnation [17–19], ion exchange with metal precursors [19–21], the adsorption

* Corresponding author. Tel.: +36 62 544207; fax: +36 62 544200.
E-mail address: mastalir@chem.u-szeged.hu (Á. Mastalir).

1381-1169/$ – see front matter © 2006 Elsevier B.V. All rights reserved.
doi:10.1016/j.molcata.2006.09.021

of molecular cluster precursors [22] and photocatalytic reduction [23]. The formation of noble metal nanoparticles inside the mesopores of MCM-41 has also been described [24–26]. As reported by Niederer et al., [27] the synthesis of MCM-41 in the presence of colloidal surfactant-stabilized noble metal nanoparticles resulted in the appearance of isolated metal clusters in the mesopores. Nevertheless, the application of such particles in catalytic reactions is far less common than that of MCM-41-supported metal nanoclusters. Recently, Pd–MCM-41 materials, with particles incorporated in the mesoporous structure, have been investigated for alkene hydrogenations [25,27] and Pd–MCM-41 samples with similar structures have been studied for the enantioselective hydrogenation of ethyl pyruvate [28].

The aim of the present study was the in situ generation of surfactant-stabilized Pd nanoparticles in MCM-41. The effect of the variation of the synthesis steps on the formation and the size distribution of the Pd particles was investigated. The Pd–MCM-41 samples were tested as catalysts for the liquid-phase hydrogenations of terminal and internal alkynes under mild conditions.

2. Synthesis strategy

As reported by Attard et al., [29] regular mesoporous nanostructures are formed via the sol–gel synthesis of silicates in bulk lyotropic liquid crystals, consisting of ordered surfactant aggregates in a suitable solvent, mostly water. The water-soluble inorganic monomer is dissolved in the aqueous domains of the organic surfactant molecules. In the synthesis gel of MCM-41, the inorganic precursor molecules of the silica framework are evenly distributed in the hexagonal phase of rod-like surfactant micelles of alkyltrimethylammonium bromides (C_nTABr; $n = 8–18$) [14,15] and the solid inorganic network around the micellar template is generated by hydrolysis of the precursor compound. Upon hydrothermal treatment, well-ordered pores are formed and then the surfactant molecules can be removed from the pores by either Soxhlet-extraction or thermal decomposition [30,31]. As the pore size of the mesoporous structure increases with the cross-sectional diameter of the template rods, the pore diameter of MCM-41 can be controlled by changing the alkyl chain length of the surfactant molecules [1–3,32] and also by solubilization of suitably selected organic guest species, including swollen micelles [1,2].

In a previous study, Pd nanoparticles have been synthetized from the precursor $K_2[PdCl_4]$, dissolved in a concentrated micellar solution of C_nTABr [31]. In the presence of a large excess of Br^-, originating from the counterions of the surfactant molecules $[PdCl_4]^{2-}$ is transformed to $[PdBr_4]^{2-}$. This ligand-exchange reaction is followed by the formation of $[C_nTA]_2[PdBr_4]$ stoichiometric complex-surfactant aggregates, which subsequently undergo solubilization to form palladate-surfactant metallomicelles [33]. Reduction of Pd(II) to Pd(0) in these metallomicelles ensures rapid adsorption of the surfactant molecules on the surface of the nascent particles, and a protective bilayer appears, leading to the formation of a Pd hydrosol with long-term stability. The Pd nanoparticles obtained by this procedure are fairly monodispersed and their mean particle diameters are 1.5–7 nm. The particle size can be controlled by varying the length of the alkyl chain, the precursor concentration and the surfactant concentration.

According to the above considerations, the synthesis strategy of Pd–MCM-41 applied in the current study involved a systematic combination of the surfactant-mediated synthesis of MCM-41 [2–4,9,14] with the surfactant-controlled synthesis of Pd nanoparticles [33]. The Pd–MCM-41samples were synthetized by two different methods:

1. The silica precursor was added to a Pd hydrosol stabilized by $C_{14}TABr$, followed by hydrolysis of the silica compound, which proceeded in a concentrated surfactant solution, in the presence of the Pd particles. This way, the Pd nanoparticles were incorporated in the silica framework upon its formation. After hydrolysis has been completed, the reaction mixture was subjected to hydrothermal treatment and the surfactant template was removed by Soxhlet-extraction.
2. The silica precursor was added to $[C_nTABr]_{mic}\cdot[C_nTA]_2[PdBr_4]$ metallomicelles, the precursor species of the Pd nanoparticles. Hydrolysis of the silica precursor was performed in a concentrated surfactant solution containing these metallomicelles. After complete hydrolysis, the Pd(II) species in the template were reduced to produce Pd(0) particles in the silica mesophase. Similarly to method 1, this procedure was also terminated by hydrothermal treatment and removal of the surfactant molecules by Soxhlet-extraction.

Both syntheses resulted in the in situ formation of Pd particles in MCM-41. The major difference between methods 1 and 2 was that the Pd nanoparticles were generated before and after formation of the silica framework, respectively. The other synthesis steps and the overall composition of the reaction mixtures were similar for the two procedures.

3. Experimental

3.1. Preparation of Pd–MCM-41 (Pd-A)

About 14.4 g of tetradecyltrimethylammonium bromide ($C_{14}TABr$, an Aldrich product) was dissolved in 80 cm^3 of distilled water and then thoroughly mixed with 30 cm^3 of an aqueous solution of $K_2[PdCl_4]$ (0.8%, 0.075 g Pd), to produce the red, water-insoluble salt $[C_nTA]_2[PdBr_4]$. Overnight stirring of the micellar system resulted in solubilization of this salt in the surfactant micelles, whereby a dark-orange transparent solution, consisting of $[C_nTABr]_{mic}\cdot[C_nTA]_2[PdBr_4]$ metallomicelles, was obtained. Upon introduction of an excess of reducing agent (5 cm^3, 5 M hydrazine in water, Fluka) into the reaction system, the colour of the micellar solution turned to dark brown, indicating the formation of Pd nanoparticles. Afterwards, 18.7 g of $Na_2Si_3O_7$ solution (27% SiO_2, 5 g) was added dropwise to the Pd hydrosol. The pH of the suspension was adjusted to 10 by using a 50% H_2SO_4 solution. On addition of the inorganic silica precursor, the Pd particles were gradually

incorporated in the silica framework formed upon hydrolysis. After stirring for 4 h, the gray-brown suspension was placed in an oven and maintained at 383 K for 6 days. After hydrothermal treatment, the solid precipitate was filtrated under suction and dried. The template was removed by Soxhlet-extraction for 30 h, with a mixture of methanol:cc HCl = 30:1. After filtration and washing, the sample was dried and stored in a vacuum desiccator. The Pd content of this material proved to be 1.47% from ICP-AES analysis.

3.2. Preparation of Pd–MCM-41 (Pd-B)

About 14.4 g of C_{14}TABr was dissolved in 100 cm^3 of distilled water (>100 times the cmc), followed by the addition of 10 cm^3 of an aqueous solution of $K_2[PdCl_4]$ (0.8%, 0.026 g Pd), which resulted in the precipitation of a red organic salt $[C_nTA]_2[PdBr_4]$. Upon vigorous stirring, solubilization of the organic salt occured, producing a quasi-homogeneous micellar solution. The formation of $[C_nTABr]_{mic}\cdot[C_nTA]_2[PdBr_4]$ metallomicelles was indicated by a deepening of the dark-orange colour observed initially. Then, 18.7 g of $Na_2Si_3O_7$ solution (27% SiO_2, 5 g) was added dropwise to the micellar solution, which led to the formation of a pale-yellow suspension. The suspension was set to pH 10 with a 50% H_2SO_4 solution. After stirring for 6 h, an excess of hydrazine hydrate (2 cm^3, 5 M in water) was introduced into the reaction system. The colour of the suspension turned to gray-brown in a few minutes, indicating that reduction of Pd(II) to Pd(0) took place. The suspension was subsequently stored in an oven at 383 K for 6 days. After hydrothermal treatment, the solid precipitate was purified in the same way as for sample A. The Pd content of the sample was found to be 0.50% by ICP-AES.

3.3. Preparation of MCM-41 (C)

In a blank experiment, MCM-41 was synthetized in the absence of Pd, under otherwise the same conditions as those for Pd-A and Pd-B.

3.4. Characterization

The Pd contents of the samples were determined by inductively coupled plasma atomic emission spectroscopy (ICP-AES), using a Jobin Yvon 24 sequential ICP-AES spectrometer at 229.7 and 324.3 nm. Before analysis, the samples were dissolved in a 1:2 mixture of aqua regia and 0.5 M $(NH_4)HF_2$ at 333 K for 24 h. The Pd loadings were obtained from the emission intensities by means of a calibration curve.

N_2 sorption measurements were performed after degassing the samples at 13 Pa and 393 K for 12 h, using a Micromeritics 2375 BET apparatus at 77 K. The specific surface areas were calculated from the BET equation and the total pore volume V_t was obtained from the amount adsorbed at the relative pressure of 0.99 [32,34,35]. Accordingly, the average pore diameters were determined as $4V_t/As_{BET}$ [4].

H_2 and CO adsorption measurements were carried out in the same apparatus which was used for N_2 sorption studies. The samples were pretreated in a H_2 atmosphere of 67 kPa at 373 K for 1 h, followed by evacuation at 413 K for 3 h. Measurements were made in the scan mode up to 1.33 kPa. CO adsorption was studied at 298 K and H_2 adsorption was measured at 333 K, to minimize β-hydride formation [36]. The dispersion of the Pd particles was determined from the H/Pd and the CO/Pd ratios extrapolated to zero pressure (chemisorption), by using the generally accepted 1:1 adsorption stoichiometries for both H/Pd and CO/Pd [37,38].

X-ray diffraction (XRD) patterns were obtained with a Philips PW 1820 diffractometer operated at 40 kV and 35 mA (Cu Kα radiation, λ = 0.154 nm). Diffraction data were collected in the range $1^\circ < 2\Theta < 6^\circ$ at an interval of 0.01 2Θ. The interplanar spacing of the MCM-41 structure (d_{100}) was calculated from the first order Bragg reflections using a PW 1877 automated powder diffraction software. The lattice parameter a, regarded as the average distance between two neighbouring pore centres in the MCM-41 structure [6], was calculated as $a = d_{100}(2/\sqrt{3})$ [4,6,30]. The average pore diameter d_p was obtained as $d_p = a - 1$, by assuming a pore wall thickness of 1 nm [3,4].

TEM images were recorded with a Philips C 10 transmission electron microscope (LaB_6 cathode, 100 kV) equipped with a Megaview II digital camera. The samples suspended in ethanol were mounted on Formvar-coated copper grids and then the solvent was evaporated. The size distribution of the particles was determined using the UTHSCSA Image Tool program and the mean particle diameters d were calculated as number average values $\left(\sum n_i d_i / \sum n_i\right)$, for at least 250 particles.

3.5. Catalytic test reaction

The liquid-phase hydrogenations of the reactants 1-pentyne, 1-hexyne and 3-hexyne (all Aldrich products of 99% purity) were investigated in an automated vibration reactor equipped with a pressure regulator, which ensured that the reactions proceeded at a constant hydrogen pressure of 10^5 Pa [39]. The mass of catalyst was 3×10^{-3} g, the reaction temperature was 298 K and the reactant:Pd ratio was S:Pd = 1000 for each measurement. The sample was pretreated in 10^5 Pa of static H_2 for 60 min. After evacuation and reintroduction of H_2, 1 cm^3 of toluene was added and pretreatment was completed under an efficient stirring for 45 min. The hydrogenation reaction was initiated by injecting the reactant into the reactor and vigorous stirring (1400 rpm) was maintained throughout the reaction to eliminate mass transport limitations. As the reaction progressed, the H_2 consumption was monitored at a data collection frequency of 0.5 s^{-1}. The reaction products were analyzed by a HP 5890 gas chromatograph equipped with a DB-1 capillary column and a flame ionization detector (FID). The catalytic activities were characterized by the initial reaction rates and the turnover frequencies (TOF).

4. Results and discussion

The N_2 sorption isotherms of the Pd–MCM-41 samples (Fig. 1a and b) correspond to type IV according to the IUPAC classification. The adsorption and the desorption pathes coincided for both samples and no hysteresis loops could be

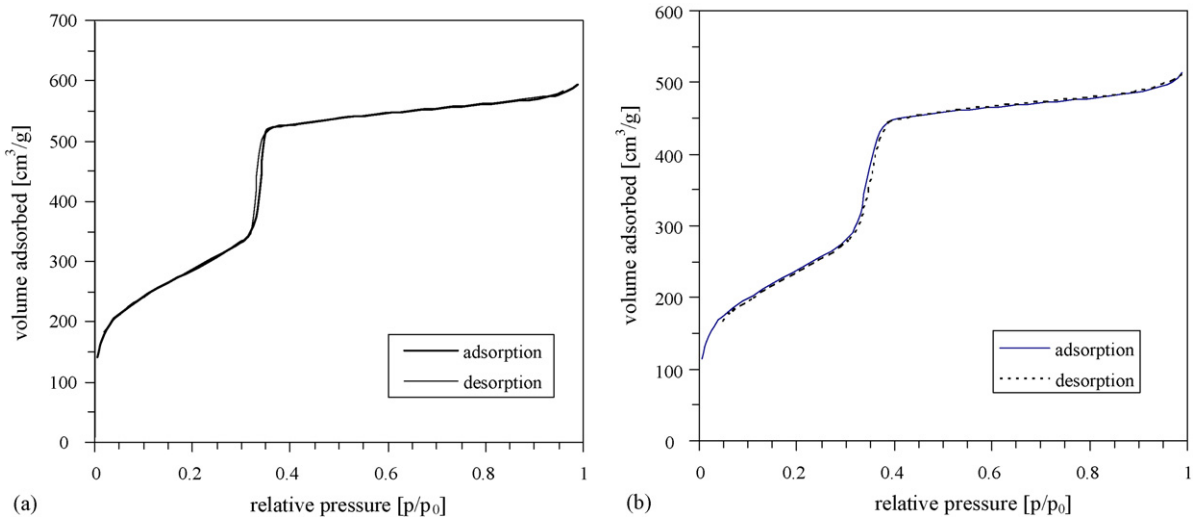

Fig. 1. (a and b) N_2 sorption isotherms of Pd-A (a) and Pd-B (b).

observed, which is in accordance with previous data reported in the literature for C_{14}–MCM-41 materials [3,4,6].

There was a sharp increase in the N_2 uptake over a narrow range of relative pressure, arising from the capillary condensation of N_2 inside the primary mesopores. The steep adsorption and desorption branches indicated a narrow mesopore size distribution [40]. In the pressure range where the primary mesopores were essentially filled with the condensed adsorbate, the plots levelled off. Secondary mesopores were not detected. The finding that the position of the capillary condensation step was the same for both samples ($p/p_0 = 0.34$) indicated a similar pore diameter [32,41]. Further, the somewhat higher steepness of the condensation step for Pd-A suggested a slightly higher uniformity of the pore sizes as compared with Pd-B [34].

XRD analysis (Fig. 2) revealed four characteristic Bragg reflections at small diffraction angles ($2\Theta = 2$–8°), which can be indexed in a hexagonal lattice and correspond well to the hexagonally arranged pore structure of MCM-41 [1], indicating long-range orders for both Pd–MCM-41 materials [6,9].

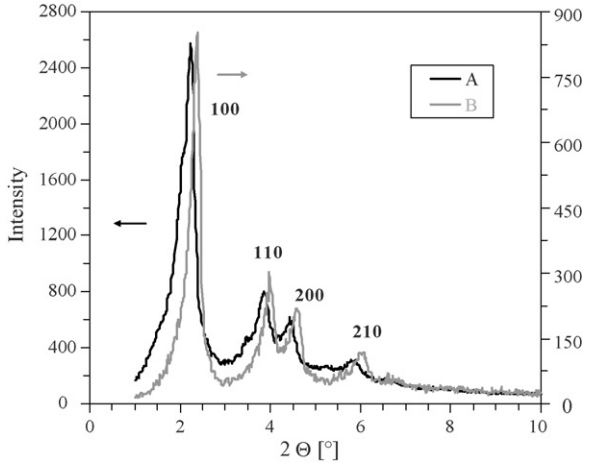

Fig. 2. X-ray diffraction patterns of the Pd–MCM-41 samples.

The arrangement and the size distribution of the Pd crystallites in the Pd–MCM-41 materials have been investigated by TEM measurements. Fig. 3 displays the TEM image of Pd-A, for which the particles were generated before formation of the MCM-41 framework. It may be observed for this sample that spherically shaped particles were formed. There is no evidence of Pd encapsulation inside the mesopores, as the particles are situated on the external surface of MCM-41. Although the location of the particles appears to be random at first sight, a closer look reveals a regular arrangement for several Pd clusters, which may be attributed to the ordered mesoporous framework of the MCM-41 host material.

The TEM images obtained for Pd-B, for which the Pd particles were generated after formation of the MCM-41 structure,

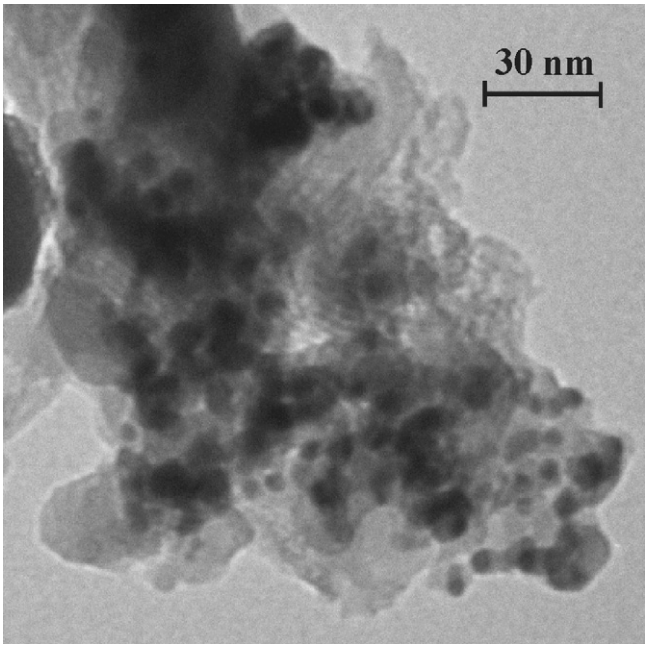

Fig. 3. Transmission electron micrograph of Pd-A.

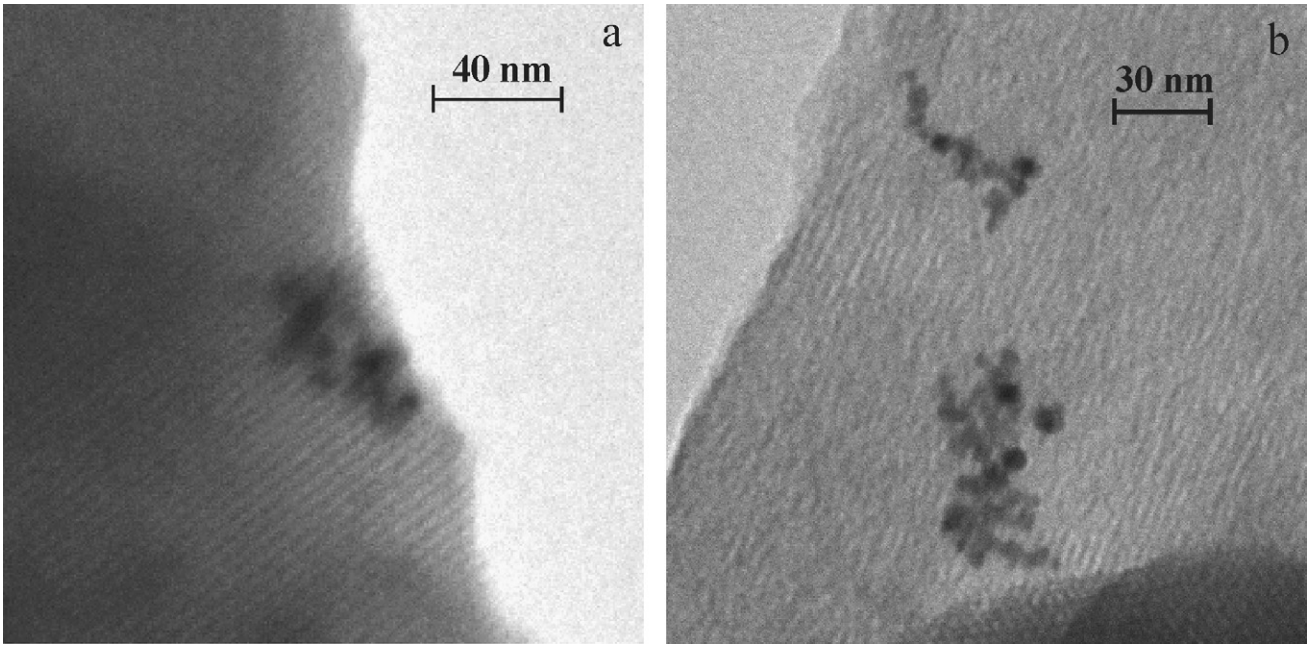

Fig. 4. (a and b) Transmission electron micrographs of Pd-B.

are demonstrated in Fig. 4. The regular pore structure of MCM-41 can be clearly distinguished in both images. It may also be seen that the Pd particle size is comparable with the pore diameter of the host material. In Fig. 4a, a relatively low contrast for the Pd particles can be observed, which may be regarded as an indication of Pd encapsulation inside the mesopores. This is also suggested by the directed arrangement of the Pd crystallites: they are oriented in the same way as the channels of MCM-41. The typically elongated particle shape equally refers to encapsulation. It follows that the Pd nanoparticles of Pd-B are incorporated in the mesoporous host material.

Although the Pd particle size range was the same (1–7 nm) for both Pd–MCM-41 samples, the size distributions were significantly different (Fig. 5a and b). For Pd-A, 70% of all the particles fell in the range 2–4 nm, whereas the frequency of particles smaller than 2 nm and larger than 4 nm was considerably lower. For Pd-B, the majority of the Pd crystallites were equally between 2 and 4 nm, but the number of Pd clusters smaller than 2 nm was considerably higher than that for Pd-A. The frequency of 4–5 nm crystallites was of a similar order, whereas the number of aggregates larger than 5 nm was insignificant. Despite the difference in the size distributions, the mean particle diameters for Pd-A and Pd-B proved to be very close values, 3.24 and 3.35 nm, respectively. It may therefore be established from TEM measurements that both synthesis methods afforded a similar size control for the Pd particles, by preventing the formation of large

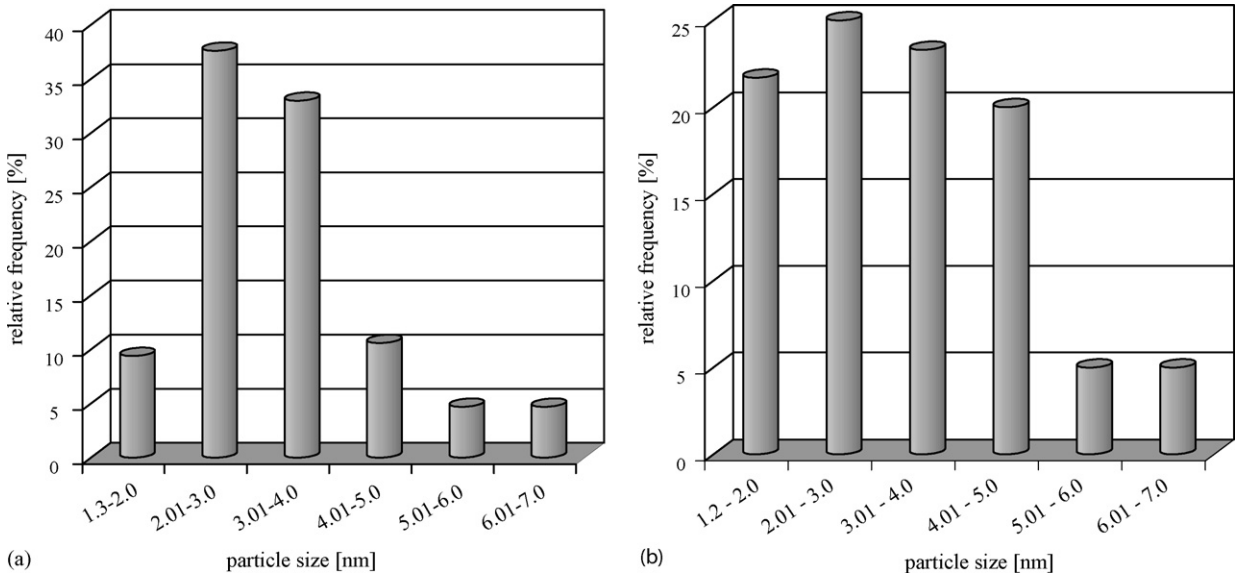

Fig. 5. (a and b) Particle size distributions of Pd-A (a) and Pd-B (b).

Table 1
Structural characterization of the Pd–MCM-41 samples

Sample	Pd (%)	As_{BET} ($m^2\ g^{-1}$)	d_{100} (nm)[a]	d_p (nm)[b]	d_p (nm)[c]	V_t ($cm^3\ g^{-1}$)[d]
Pd-A	1.47	876	4.08	3.62	3.71	0.79
Pd-B	0.5	1037	3.78	3.54	3.36	0.92
C	–	1042	3.98	4.17	3.60	1.09

[a] Periodicity of the MCM-41 host, determined from XRD data.
[b] Average pore diameter, obtained as $4V_t/As_{BET}$.
[c] Average pore diameter, calculated from XRD data as $d_p = d_{100}\ (2/\sqrt{3}) - 1$.
[d] Total pore volume.

Pd aggregates. Nevertheless, the sequence of the synthesis steps (reduction of Pd(II) and formation of the MCM-41 framework) was found to have a crucial effect on both the location and the size distribution of the Pd particles. The results obtained from the structural characterization of the Pd–MCM-41 samples are listed in Table 1.

The specific surface area of Pd-B was very close to that of pure MCM-41, whereas that of sample A was somewhat lower, indicating a slightly less ordered structure [6,42], which was also detected by TEM. Nevertheless, all the structural parameters of the Pd-containing samples proved to be very similar to that of pure MCM-41. Hence, it may be pointed out that, irrespective of the preparation procedure, the formation of the Pd nanoparticles exerted no significant influence on the highly ordered structure of the host material [26]. It should also be emphasized that the average pore diameters determined from N_2 sorption were in good agreement with those calculated from XRD data [4]. Further, both values are comparable with the mean particle diameters.

The Pd dispersions, obtained from both H_2 and CO chemisorption measurements, are displayed in Table 2. The dispersion values were also cross-checked by TEM [36].

It may be observed from Table 2 that the dispersions obtained by adsorption techniques were remarkably close and only slightly higher than those calculated from the mean particle diameters. Accordingly, the average of the dispersion values determined experimentally (0.37 and 0.35 for Pd-A and Pd-B, respectively) was used for further calculations.

Table 2
Dispersions of the Pd–MCM samples obtained by different methods

Sample	D_{H2}	D_{CO}	D_{TEM}[a]	d_{TEM} (nm)
Pd-A	0.39	0.34	0.31	3.24
Pd-B	0.32	0.38	0.30	3.35

[a] $D_{TEM} = 1.00/d_{TEM}$ [36].

As related to a favourable combination of activity and selectivity, Pd has long been regarded as the most efficient metal for alkyne hydrogenation [45,46]. This reaction is typically regarded as structure insensitive [45,46], although recent studies disclosed a structure sensitivity at high Pd dispersions [44,47]. The first reaction investigated over the Pd–MCM-41 samples was the selective hydrogenation of 1-pentyne, for which the main reaction product was 1-pentene. As shown in Fig. 6a and b, the H_2 consumption was monitored as a function of the reaction time. For Pd-A, a typical zero order reaction was observed, which is characteristic of alkene and alkyne hydrogenation over supported metal catalysts [18,48,49]. The initial rate was maintained as the reaction progressed, indicating that the active centres were readily accessible for the reactant molecules [50]. Recently, similar observations have been made for the hydrogenation of phenylacetylene and 1-phenyl-1-hexyne over Pd particles supported on mesostructured silicas [51]. The linear trend of the hydrogenation rate is in accordance with the result of TEM measurements, which revealed the occur-

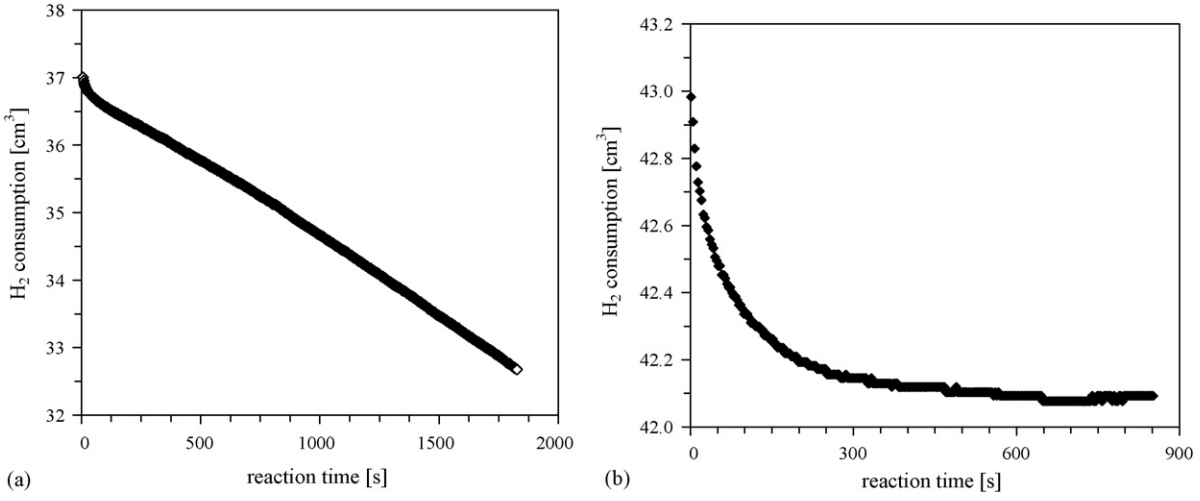

Fig. 6. (a and b) Hydrogenation of 1-pentyne over Pd-A (a) and Pd-B (b) $m = 5 \times 10^{-3}$ g, S:Pd = 1000, $p = 10^5$ Pa, $T = 298$ K and solvent: 1 cm^3 of toluene.

Table 3
Hydrogenation of terminal alkynes over Pd–MCM-41 catalysts

Sample[a]	Reactant	Reaction rate (cm^3 H_2 min^{-1} g Pd^{-1})	TOF (s^{-1})	Conversion (%)[b]	Selectivity (%)[b]
Pd-A	1-Pentyne	4,927	0.97	55.5	100
Pd-B	1-Pentyne	35,333	7.32	38.1	100
Pd-A	1-Hexyne	6,369	1.25	33.3	100
Pd-B	1-Hexyne	26,853	5.56	8.7	100

[a] $m = 5$ mg, $T = 298$ K, $p = 10^5$ Pa and S:Pd = 1000.
[b] Reaction time: 30 min.

rence of quasi-spherical Pd particles on the external surface of MCM-41.

On the other hand, the catalytic behaviour of Pd-B proved to be completely different. As may be observed in Fig. 6b, the high initial rate declined rapidly after a few minutes and then the reaction slowed down considerably. This trend may be attributed to the effect of mass transport limitations, as related to the encapsulation of Pd particles in the mesoporous structure. Such particles can only be accessed by diffusion of the reactant molecules inside the mesopores, which tends to have a limiting effect on the reaction rate. Similar results have been obtained for the hydrogenation of phenylacetylene over clay-intercalated Pd nanoparticles [39]. As revealed in Fig. 6a and b, the Pd particles incorporated in MCM-41 are clearly less accessible for the reactant molecules than those exposed on the surface of the host material. It follows that the actual Pd dispersion of Pd-B must be significantly lower than that obtained from the mean particle diameter. The decreasing trend observed for the H_2 consumption over Pd-B may also be regarded as an indirect evidence that this sample contains no external Pd crystallites on the surface of MCM-41. The results obtained for the catalytic hydrogenations of 1-pentyne and 1-hexyne over the Pd–MCM-41 samples are summarized in Table 3.

The initial turnover frequencies, calculated from the initial hydrogenation rates, proved to be significantly higher for Pd-B for both reactants. Nevertheless, given the significant decrease of the reaction rate observed for this sample, the catalytic activities may be more adequately characterized by the conversions at the same reaction time. It may therefore be established that Pd-A was a more active catalyst for both reactants. The activity difference proved to be more pronounced for 1-hexyne, whereas the alkene selectivity was 100% in all cases.

It should be emphasized that the catalytic behaviour of Pd-B is in contradiction with the results of previous studies, which reported substantial catalytic activities for noble metal particles, claimed to be encapsulated in MCM-41, for either alkene or ethyl pyruvate hydrogenations [17,27,28]. However, for these studies, encapsulation of the noble metal particles has not been confirmed by TEM images and hence the catalytic performance of such materials may be related to the presence of surface metal clusters [17,28].

The catalytic performances of the Pd–MCM-41 samples were also examined for the hydrogenation of an internal alkyne, 3-hexyne. As reported in the literature, the stereoselective hydrogenation of internal alkynes typically results in the predominant formation of the (*Z*)-alkene stereoisomer [43,52]. For the liquid-phase hydrogenations of lower alkynes, the (*Z*)-alkene stereoselectivities have been found to exceed the selectivities of terminal alkenes, obtained from monosubstituted acetylenes [52]. The H_2 consumptions detected for the two samples are displayed in Fig. 7a and b. Similarly to that observed for terminal alkynes, hydrogenation proceeded with a constant rate for Pd-A, whereas for Pd-B, a decreasing trend could be observed. Nevertheless, the decline for 3-hexyne over Pd-B was less pronounced than those for terminal alkynes. Fig. 7a also demonstrates the reproducibility of the measurement, as the two plots were obtained from independent runs. The hydrogenation rates were determined from the slopes, which proved to be very similar. The compositions of the product mixtures obtained for the hydrogenation of 3-hexyne are listed in Table 4.

Despite the high initial rate and turnover frequency observed for Pd-B, the conversion for Pd-A proved to be considerably higher, indicating that the latter sample was a more active catalyst. Nevertheless, there was practically no difference between the product selectivities, which is in accordance with the results of our previous studies [53]. The main reaction product was the (*Z*)-alkene, and only very small amounts of (*E*)-alkene and alkane were detected. The selectivities of the by-products were of the same order. As related to the similar Pd particle diameters obtained for both Pd–MCM-41 samples, the remarkably high *Z* stereoselectivities (>94%) may be attributed to the predominance of terrace surface sites, which have been reported to be

Table 4
Hydrogenation of 3-hexyne over Pd–MCM-41 catalysts

Catalyst[a]	Reaction rate (cm^3 H_2 min^{-1} g Pd^{-1})	TOF (s^{-1})	Conversion (%)[b]	Selectivity (%)[b]		
				Z	*E*	Alkane
Pd-A	5,848	1.15	46.3	94.2	4.2	1.6
Pd-B	25,793	5.34	8.2	94.5	4.4	1.1

[a] $m = 5$ mg, $T = 298$ K, $p = 10^5$ Pa and S:Pd = 1000.
[b] Reaction time: 30 min.

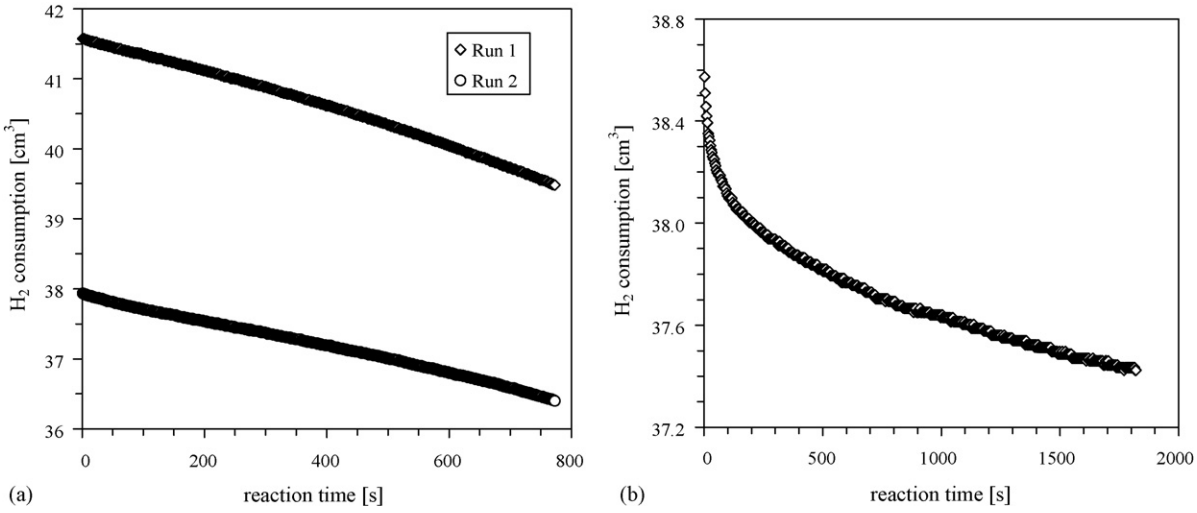

Fig. 7. (a and b) Hydrogenation of 3-hexyne over Pd-A (a) and Pd-B (b) $m = 5 \times 10^{-3}$ g, S:Pd = 1000, $p = 10^5$ Pa, $T = 298$ K and solvent: 1 cm^3 of toluene.

the most selective surface structure of fcc Pd nanoparticles [54]. In this respect, the significant (*Z*) stereoselectivity of 3-hexyne hydrogenation tends to originate from the decreased hydrogenation rate of the (*Z*)-alkene, due to a relatively low-energy Pd surface [55], rather than from alkyne overhydrogenation [54].

For Pd-A, which proved to be a more efficient catalyst, the product selectivities of 3-hexyne hydrogenation were also investigated as a function of the reaction time (Fig. 8). For the stereoselectivity of the (*Z*)-alkene formation, only a minor decrease could be observed as the reaction progressed. Hexane was an initial product [42] and the low extent of overhydrogenation displayed no variation up to 50 min. The small amount of (*Z*)-3-hexene was formed both directly [56] and through $Z \rightarrow E$ isomerization [57]. As the total amount of the by-products did not exceed 7%, the pronounced (*Z*) stereoselectivity of Pd-A was essentially maintained throughout the reaction.

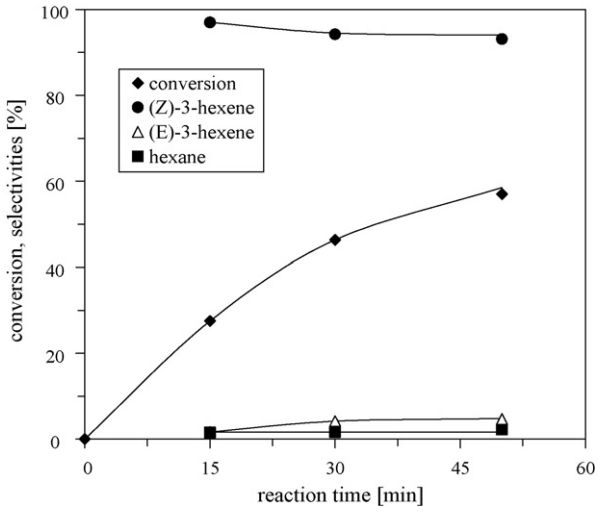

Fig. 8. Reaction time dependence of the conversion and the product selectivities for the hydrogenation of 3-hexyne over Pd-A $m = 5 \times 10^{-3}$ g, S:Pd = 1000, $p = 10^5$ Pa, $T = 298$ K and solvent: 1 cm^3 of toluene.

5. Conclusions

Pd–MCM-41 samples were prepared by a novel synthesis method, based on a systematic combination of the surfactant-mediated formation of MCM-41 and the in situ generation of surfactant-stabilized Pd nanoparticles. Pd nanoparticles were obtained by the reduction of $K_2[PdCl_4]$, both before and after formation of the MCM-41 framework.

Structural characterization of the Pd–MCM-41 samples gave evidence that the presence of the Pd particles had no decreasing effect on the pronounced structural order of MCM-41. On the other hand, the variation in the sequence of the synthesis steps resulted in significant differences between the location and the size distribution of the Pd particles. For Pd-A, for which the particles were generated before formation of the MCM-41 structure, spherically shaped Pd nanoparticles were detected on the external surface of MCM-41. This sample may therefore be regarded as an MCM-41-supported Pd catalyst. In contrast, the Pd particles of Pd-B, obtained after formation of the MCM-41 framework, were found to be encapsulated inside the mesopores.

It was pointed out that the Pd particles incorporated in MCM-41 were significantly less active in liquid-phase alkyne hydrogenation than those on the external surface of the mesoporous host. This finding can be attributed to limited access of the reactants to the active centres situated in the mesoporous framework channels. It is therefore suggested that the hydrogenation rate observed for Pd-B is restricted by mass transport limitations. Nevertheless, despite the difference in the catalytic activities, the selectivities of the Pd–MCM-41 samples proved to be very similar, as both samples displayed remarkably high (*Z*) stereoselectivities for the hydrogenation of 3-hexyne.

Acknowledgement

Financial support through OTKA Grants T 047390, T 042603 and the Bolyai János Research Foundation is gratefully acknowledged.

References

[1] C.T. Kresge, M.E. Leonowitz, W.J. Roth, J.C. Vartuli, J.S. Beck, Nature 359 (1992) 710–712.
[2] A. Taguchi, F. Schüth, Micropor. Mesopor. Mater. 77 (2005) 1–45.
[3] C.G. Sonwane, S.K. Bhatia, Langmuir 15 (1999) 2809–2816.
[4] M. Grün, K.K. Unger, A. Matsumoto, K. Tsutsumi, Micropor. Mesopor. Mater. 27 (1999) 207–216.
[5] M. Kruk, M. Jaroniec, A. Sayari, Langmuir 13 (1997) 6267–6273.
[6] M. Broyer, S. Valange, J.P. Bellat, O. Bertrand, G. Weber, Z. Gabelica, Langmuir 18 (2002) 5083–5091.
[7] A. Sayari, Chem. Mater. 8 (1996) 1840–1852.
[8] S. Ernst, M. Selle, Micropor. Mesopor. Mater. 27 (1999) 355–363.
[9] A. Corma, Topics Catal. 4 (1997) 249–260.
[10] F.A. Twaiq, A.R. Mohamed, S. Bhatia, Micropor. Mesopor. Mater. 64 (2003) 95–107.
[11] B.G. Johnson, C.H. Bartholomew, D.W. Goodman, J. Catal. 128 (1991) 231–247.
[12] A. Bhaumik, T. Tatsumi, J. Catal. 189 (2000) 31–39.
[13] B. Solsona, T. Blasco, J.M. Lopez Nieto, M.L. Pena, F. Rey, A. Vidal-Moya, J. Catal. 203 (2001) 443–452.
[14] D.M. Antonelli, J.Y. Ying, Curr. Opin. Colloid Surf. Sci. 1 (1996) 523–529.
[15] C.G. Göltner, M. Antonietti, Adv. Mater. 9 (1997) 431–436.
[16] P.T. Tanev, T.J. Pinnavaia, Science 267 (1995) 865–867.
[17] C.A. Koh, R. Nooney, S. Tahir, Catal. Lett. 47 (1997) 199–203.
[18] J. Panpranot, K. Pattamakomsan, J.G. Goodwin Jr., P. Prasertham, Catal. Commun. 5 (2004) 583–590.
[19] U. Junges, W. Jacobs, I. Voigt-Martin, B. Krutzsch, F. Schüth, J. Chem. Soc. Chem. Commun. (1995) 2283–2284.
[20] B.M. Choudary, K.L. Kantam, N.M. Reddy, K.K. Rao, Y. Haritha, V. Bhaskar, F. Figueras, A. Tuel, Appl. Catal. A 181 (1999) 139–144.
[21] M. Hartmann, C. Bischof, Z. Luan, L. Kevan, Micropor. Mesopor. Mater. 44/45 (2001) 385–394.
[22] S. Behrens, G. Spittel, Dalton Transactions 5 (2005) 868–873.
[23] S. Zheng, L. Gao, Mater. Chem. Phys. 78 (2) (2003) 512–517.
[24] X.G. Zhao, J.L. Shi, B. Hu, L.X. Zhang, Z.L. Hua, Mater. Lett. 58 (2004) 2152–2156.
[25] S.H. Choi, J. Ind. Eng. Chem. 10 (2004) 1015–1024.
[26] Z. Kónya, V.F. Puntes, I. Kiricsi, J. Zhu, P. Alivisatos, G.A. Somorjai, Catal. Lett. 81 (2002) 137–140.
[27] J.P.M. Niederer, A.B.J. Arnold, W.F. Hölderich, B. Spliethof, B. Tesche, M. Reetz, H. Bönnemann, Topics Catal. 18 (2002) 265–270.
[28] T.J. Hall, J.E. Halder, G.J. Hutchings, R.L. Jenkins, P. Johnston, P. McMorn, P.B. Wells, R.P.K. Wells, Topics Catal. 11 (2000) 351–357.
[29] G.S. Attard, J.C. Clyde, C.G. Göltner, Nature 378 (1995) 366–368.
[30] M. Kruk, M. Jaroniec, R. Ryoo, S.H. Joo, Chem. Mater. 12 (2000) 1414–1421.
[31] K. Moller, T. Bein, R.X. Fischer, Chem. Mater. 11 (1999) 665–673.
[32] M. Kruk, M. Jaroniec, R. Ryoo, C. Hyun Ko, J. Phys. Chem. B 104 (2000) 292–301.
[33] B. Veisz, Z. Király, Langmuir 19 (2003) 4817–4824.
[34] J. Choma, S. Pikus, M. Jaroniec, Appl. Surf. Sci. 252 (2005) 562–569.
[35] K.S.W. Sing, D.H. Everett, R.A. Haul, L. Moscou, R.A. Pirotti, J. Rouquerol, T. Siemieniewska, Pure Appl. Chem. 57 (1985) 603–619.
[36] W. Zou, R.D. Gonzalez, Catal. Lett. 12 (1992) 73–86.
[37] N. Krishnankutty, M.A. Vannice, J. Catal. 155 (1995) 312–326.
[38] J.E. Benson, H.S. Hwang, M. Boudart, J. Catal. 30 (1973) 146–153.
[39] Á. Mastalir, Z. Király, J. Catal. 220 (2003) 372–381.
[40] C. Yang, P. Liu, Y. Ho, C. Chiu, K. Chao, Chem. Mater. 15 (2003) 275–280.
[41] M.J. Meziani, J. Zajac, D.J. Jones, J. Roziere, S. Partyka, Langmuir 13 (1997) 5409–5417.
[42] A. Papp, Á. Molnár, Á. Mastalir, Appl. Catal. A 289 (2005) 256–266.
[43] S. Bailey, F. King, in: R.A. Sheldon, H. van Bekkum (Eds.), Fine Chemicals through Heterogeneous Catalysis, Wiley, New York, 2001, pp. 351–362.
[44] Á. Molnár, A. Sárkány, M. Varga, J. Mol. Catal. A: Chem. 173 (2001) 185–221.
[45] J.G. Ulan, W.F. Maier, J. Mol. Catal. 54 (1989) 243–261.
[46] G. Del Angel, J.L. Benitez, J. Mol. Catal. A: Chem. 94 (1994) 409–416.
[47] D. Duca, F. Frusteri, A. Parmaliana, G. Deganello, Appl. Catal. A 146 (1996) 269–284.
[48] G. Carturan, G. Facchin, G. Cocco, S. Enzo, G. Navazio, J. Catal. 76 (1982) 405–417.
[49] L. Guczi, Z. Schay, Gy. Stefler, L.F. Liotta, G. Deganello, A.M. Venezia, J. Catal. 182 (1999) 456–462.
[50] J. Panpranot, O. Tangjitwattakorn, P. Prasertham, J.G. Goodwin Jr., Appl. Catal. A 292 (2005) 322–327.
[51] N. Marín-Astorga, G. Pecchi, T.J. Pinnavaia, G. Alvez-Manoli, P. Reyes, J. Mol. Catal. A: Chem. 247 (2006) 145–152.
[52] H. Gutman, H. Lindlar, in: H.G. Viehe (Ed.), Chemistry of Acetylenes, Marcel Dekker, New York, 1969, pp. 355–364.
[53] Á. Mastalir, Z. Király, F. Berger, Appl. Catal. A 269 (2004) 161–168.
[54] J.G. Ulan, W.F. Maier, J. Org. Chem. 52 (1987) 3132–3143.
[55] R. van Hardeveld, F. Hartog, Adv. Catal. 22 (1972) 75–113.
[56] C.A. Henrick, Tetrahedron 33 (1977) 1845–1889.
[57] M. Bartók, Stereochemistry of Heterogeneous Metal Catalysis, Wiley, Chichester, 1985.